COMMUNICATION

Short-range ordering in battery electrode, the 'cation-disordered' rocksalt $Li_{1.25}Nb_{0.25}Mn_{0.5}O_2$

Michael A Jones,[a] Philip J Reeves,[a] Ieuan D Seymour,[a†] Matthew J Cliffe,[b] Siân E Dutton*[c] and Clare P Grey*[a]

Cation order, with a local structure related to γ-$LiFeO_2$, is observed in the nominally cation-disordered Li-excess rocksalt $Li_{1.25}Nb_{0.25}Mn_{0.5}O_2$ via X-ray diffraction, neutron pair distribution function analysis, magnetic susceptibility and NMR spectroscopy. The correlation length of ordering depends on synthesis conditions and has implications for the electrochemistry of these phases.

Improvements to the energy density of current commercial Li-ion batteries based on conventional cathode materials such as $LiCoO_2$ and $Li[NiMnCo]O_2$ (NMC) are becoming increasingly challenging to achieve.[1] Hence, new families of materials with inherently greater capacities are required.

Li-excess cation-disordered materials have shown promise as materials with significantly higher achievable capacities.[2] This extra capacity is thought to be achieved through reversible oxygen redox, in addition to traditional transition metal (TM) redox.[3–6] They allow for a broad compositional range and offer a vast, largely untapped phase space.[2,7,8] Until recently, it was thought that Li diffusion is too slow in these materials for them to be viable cathode materials. However, demonstration of a large and reversible capacity in $Li_{1.211}Mo_{0.467}Cr_{0.3}O_2$—originally layered but which rapidly forms a disordered rocksalt structure on cycling – has rekindled interest in this class of material.

The family of Li-excess materials $Li_{1+x}Nb_yM_zO_2$ (x + y + z = 1, M = V, Mn, Fe, Co, Ni) are promising new cathode materials.[2] They are solid solutions of the rocksalts Li_3NbO_4 and either $LiMO_2$ (M = V, Mn, Fe) or MO (M = Co, Ni), and have been reported to crystallise into a cation-disordered rocksalt structure. Their reversible capacities, which were demonstrated to be greater than those predicted based solely on TM redox,

earned them a great deal of attention as potentially exhibiting reversible O redox.[2] Changes in their O K-edge X-ray absorption spectra, and electron energy loss spectroscopy spectra have been put forward as evidence of O redox being responsible for this extra capacity.[9–12] The true structure of these materials is still poorly understood, leaving the structural roots of their interesting redox chemistry obscure. Li—O—Li 180° linkages, a consequence of both cation disorder and a Li:TM ratio greater that one, have been implicated as a key structural motif that yields unhybridised and readily oxidised O 2p states.[3,13,14]

Local short-range ordering has significant consequences for the Li-ion transport throughout these Li-excess structures.[15,16] Here we focus on the Mn-containing member of the family, $Li_{1.25}Nb_{0.25}Mn_{0.5}O_2$ (LNbMO). An ordering model deduced from X-ray and neutron powder diffraction data (PXRD and NPD) is proposed and rationalised based on electroneutrality.

$Li_{1.25}Nb_{0.25}Mn_{0.5}O_2$ powder was prepared by a solid state reaction at 1000°C under flowing Ar for 12 h. The cooling rate was varied by either allowing the sample to cool to room temperature inside the furnace, or removing the portion of the tube containing the sample at 1000°C to facilitate more rapid cooling whilst still under an Ar atmosphere.

Measured PXRD patterns of LNbMO—cooled at these two different rates contained significant differences. Samples which were cooled slowly exhibited an extra set of broad reflections in addition to those expected for the completely disordered rocksalt structure [Fig. 1b], whereas samples which were rapidly cooled only had very broad features in those positions [Fig. 1a]. These comparatively low intensity broad reflections were present in previously reported diffraction measurements of this material, however until now they have avoided much discussion, and have been omitted from structural refinements.[11] We found that the extra reflections can be indexed to a body centred tetragonal supercell in which $a' = b' = a_{rs}$; $c' = 2a_{rs}$ (a_{rs} is the original rocksalt lattice parameter). This unit cell accounts for all observed reflections, with selective peak broadening in the case that l is odd. This broadening associated with the peaks arising from
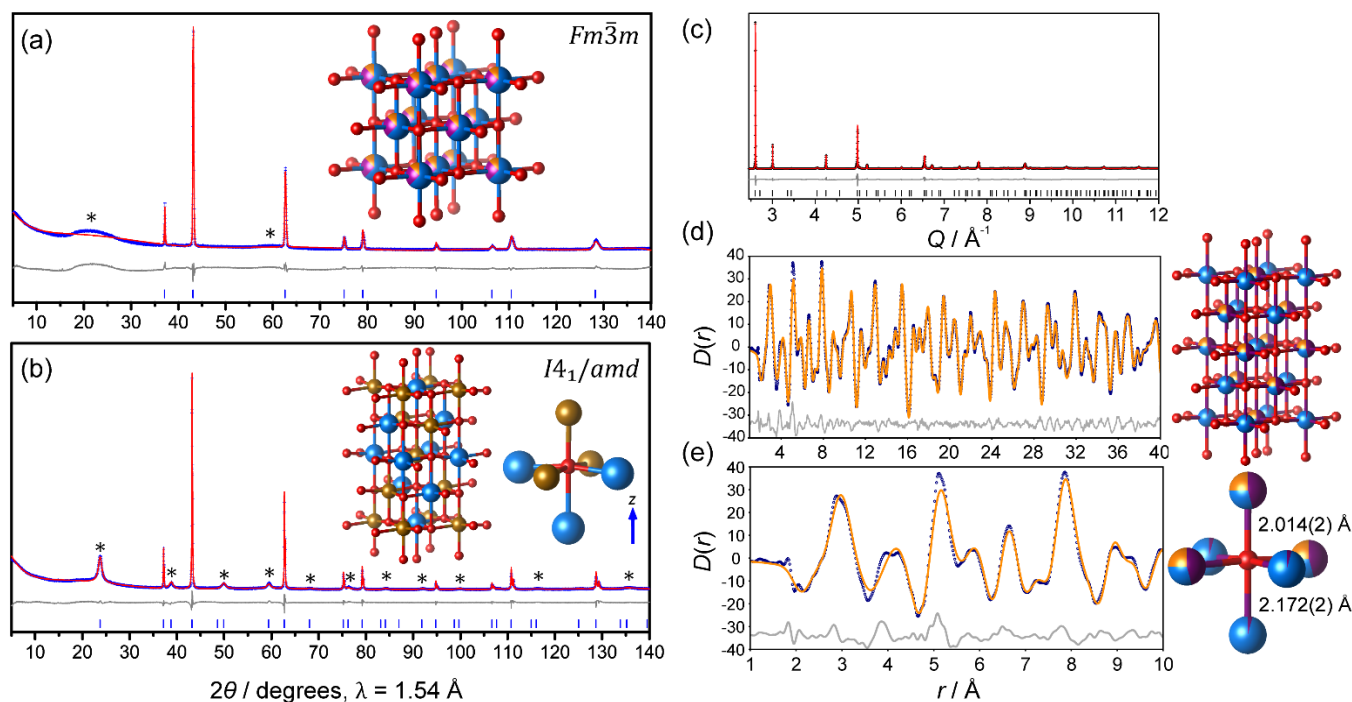
Figure 1. (a, b) PXRD data for two samples of $Li_{1.25}Nb_{0.25}Mn_{0.5}O_2$. (a) Rietveld refinement for a sample containing broad, low-intensity superstructure peaks (*). The inset shows the disordered rocksalt $Fm\bar{3}m$ unit cell, a = 4.19551(7) Å and a statistical distribution of Li (blue), Nb (orange) and Mn (purple) on the metal site. (b) Rietveld refinement for a sample containing high-intensity superstructure peaks (*), using a structural model with a body centred tetragonal unit cell in which $a' = b' = a_{rs}$; $c' = 2a_{rs}$, with space group $I4_1/amd$, a_{rs} = 4.18651(1) Å, the space group of γ-LiFeO$_2$ (shown in the inset). Neutron Bragg (c) and PDF (d, e) data for an ordered sample of LNbMO, refined (along with lab PXRD data) against a structural model based on the unit cell of γ-LiFeO$_2$ (only the highest resolution bank 5 neutron Bragg data are shown). The O coordination environment is shown (bottom-right) along with the two axial bond lengths. The experimental data are plotted as blue crosses (PXRD), black crosses (NPD) and purple open circles (PDF). The calculated values are plotted as solid red (Bragg) and orange (PDF) lines, and the difference curves as grey lines. The location of expected reflections in each case are shown by blue (PXRD) or black (NPD) tickmarks. R$_w$ = 1.930% and χ^2 = 0.035% for the combined refinement. The refinement was performed using TOPAS Academic v6.

superstructure suggest ordered domains of limited size along c: with a fitted correlation length of 125 Å (30 a_{rs}) for the slowly cooled sample, of 10 Å for the rapidly cooled sample.

It is important to note at this stage that the samples which display these additional reflections—and will be referred to herein as more ordered samples—are still fairly disordered on average. They do however exhibit correlation between metal occupancies on a length scale an order of magnitude greater than their more disordered analogues.

Symmetry analysis using the ISODISTORT software was carried out to generate the various cation-ordered superstructures consistent with the observed superlattice. We found that only one structure was consistent with the observed PXRD data, the $I4_1/amd$ γ-LiFeO$_2$ structure.[17,18] The γ-LiFeO$_2$ structure is derived from a rocksalt structure by ordering Li and Fe into two separate interpenetrating metal sublattices.[19] In the resulting tetragonal structure, each oxygen is coordinated by three metal cations from each sublattice in a meridional fashion [Fig. 1b].

To examine the nature of the LNbMO short-range ordering, pair distribution function (PDF) analysis was performed on neutron total scattering data for a slowly-cooled sample of LNbMO (i.e. with additional superstructure reflections) [Fig. 1c-e]. A combined Rietveld[20,21] refinement of neutron Bragg, PDF and laboratory XRD data was performed against a structural model with the proposed tetragonal $I4_1/amd$ space group, using the γ-LiFeO$_2$ unit cell as a starting point. The Li, Nb and Mn occupancies of the two symmetry distinct metal sublattices in the unit cell were allowed to refine separately, but were

constrained such that each metal sublattice was fully occupied (Table 1). This refinement robustly demonstrated that one sublattice is almost entirely populated with lithium [95.4(3)% Li, 4.6(5)% Mn] and the other with Mn, Nb and the remaining Li— i.e. a composition of $[Li_{0.95}Mn_{0.05}][Li_{0.30}Nb_{0.25}Mn_{0.45}]O_2$ [Fig. 1e]. The descent in symmetry to a tetragonal space group also allows the oxygen atoms to displace in the z direction. Refinement of z suggests the O moves towards the

Table 1. Crystallographic data of structural model of $Li_{1.25}Nb_{0.25}Mn_{0.5}O_2$, obtained from combined refinement of diffraction and PDF data. R$_w$ = 1.930%; χ^2 = 0.035%

Space group $I4_1/amd$ (Origin Choice 2); Z=8						
a = b = 4.185729(5) Å; c = 2a; α = β = γ = 90°						
Atom	Wyckoff position	x	y	z	B$_{iso}$	Occupancy (%)
O1	8e	0	1/4	0.1344(2)	1.42(2)	100
^{7}Li1						95.4(3)
Mn1	4a	0	3/4	1/8	1.06(3)	4.6(5)
Nb1						0.0(4)
^{7}Li2						29.6(3)
Mn2	4b	0	1/4	3/8	0.93(1)	45.4(5)
Nb2						25.0(4)

Table 2. Bond distances of refined structural model of $Li_{1.25}Nb_{0.25}Mn_{0.5}O_2$. M^{sub1} and M^{sub1} correspond to the table of crystallographic data above.

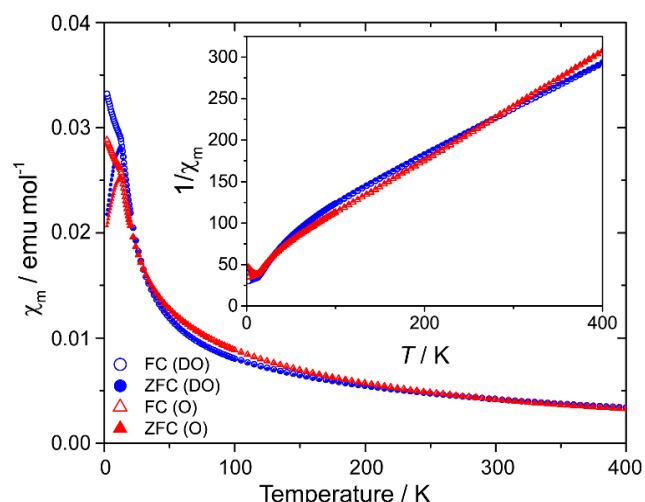| Bond	Length (Å)
Axial O—M^{sub1}	2.172(2) x 2
Axial O—M^{sub2}	2.014(2) x 2
Equatorial O—M$^{sub1\&2}$	2.09434(7) x 4

Figure 2. Magnetic susceptibility data for disordered (blue) and ordered (red) LNbMO. Curie constants of 1.8 (disordered) and 1.53 (ordered) were obtained, giving magnetic moments ($\mu_{eff} = \sqrt{8.00C}$) of 3.8 and 3.5 μ_B respectively, similar to the spin only value of 3.46 μ_B expected. Weiss temperatures of -131 K and -70 K were obtained.

predominantly transition metal sublattice, in keeping with what we would expect from simple electrostatics [Fig. 1e, Table 2]. Given this shortening of the axial Mn—O bonds and the tendency for Mn^{3+} to undergo a Jahn-Teller (JT) distortion, it is likely that a JT elongation is accommodated in the xy plane.

Having established the existence of γ-LiFeO$_2$-like ordering using diffraction, magnetometry was used to ascertain how this local ordering perturbs the electronic structure. At high temperatures, $T > 150$ K, the susceptibility, χ, of both samples [Fig. 2] could be fit using the Curie Weiss law. The Curie constants C are consistent with both LNbMO samples containing exclusively Mn^{3+}. The Weiss temperature, θ, for the more disordered sample ($\theta = -131$ K) is almost twice as negative as that of the more ordered sample ($\theta = -70$ K). These stronger antiferromagnetic interactions suggest there are a larger number of Mn-O-Mn 180° interactions, which are expected to be antiferromagnetic.[22,23] A sample with more strongly correlated ordering should contain fewer such linkages, assuming the Mn are themselves ordered within the TM sublattice to accommodate JT distortions. The broad peaks in the ZFC susceptibilities, divergence of the FC susceptibilities at 13 K and observed hysteresis in the $M(H)$ plots [Fig. S4 & S5, ESI] are indicative of spin-glass behaviour, consistent with disorder in the arrangement of Mn^{3+}.

Magic angle spinning (MAS) NMR spectra were obtained to probe lithium local environments. In these rocksalt materials, each Li ion has 12 nearest neighbour metal ions with 90° bond angles and 6 next-nearest neighbours with 180° bond angles. For completely disordered Li$_{1.25}$Nb$_{0.25}$Mn$_{0.5}$O$_2$ each of these 1st and 2nd nearest TM neighbours has a 25% probability of being paramagnetic Mn^{3+}—each Mn neighbour causing a large Fermi contact shift. The magnitude and sign of the shift depends on the nature of the bond pathway (180° or 90°),[24] resulting in a large number of different Li environments and a broad NMR spectrum. The diamagnetic Li$^+$ and Nb^{5+} neighbours do not contribute significantly to the Fermi contact shift. On increasing the local order, the probability distribution of Li nearest
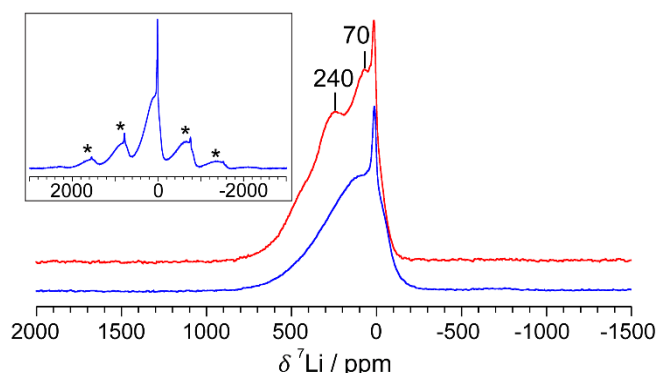

Figure 3. ^{7}Li pjMATPASS spectra of disordered (blue) and ordered (red) samples of Li$_{1.25}$Nb$_{0.25}$Mn$_{0.5}$O$_2$, scaled by mass and number of scans. The inset shows the Hahn echo spectrum with the spinning sidebands (*). The MATPASS pulse sequence is used to separate the isotropic resonance from the sideband manifold (60 kHz MAS).[28]

neighbours changes significantly. In particular, the number of probable environments is reduced, and fewer resonances are observed, as seen in the spectrum for the slowly cooled sample, where distinct broad features can be discerned around 240 and 70 ppm [Fig. 3]. A more definitive assignment of these spectra is challenging as the observed spectra will reflect not only the cation order, but also the orbital order of each Mn^{3+} neighbour. Despite this complexity, it is clear that the clustering of resonances observed in the more highly correlated sample is consistent with a greater correlation length of local ordering.

The preference for the observed γ-LiFeO$_2$ cation ordering can be understood by a tendency towards local electroneutrality.[19] Ideally each O^{2-} would experience an octahedral coordination by six cations whose charges sum to +12 (each cation is shared between six O). In this composition the available metal cations have charges of +1, +3 or +5 (Li, Mn and Nb, respectively) and so local electroneutrality can be achieved only in two ways: OLi$_3$Mn$_3$ (c.f. γ-LiFeO$_2$) or OLi$_4$NbMn. This latter scenario is most suited to the stoichiometry in this composition of LNbMO (62.5% Li, 12.5% Nb, 25% Mn), with excess Mn^{3+} accommodated via the former arrangement. In the 4:1:1 arrangement, any distribution of four Li ions will have a subset of three 'pseudo-meridional' ions and so both the 4:1:1 and 3:3 environments are consistent with the observed cation order.

Given the diversity of structures possible when two or more cations occupy the Na site of the NaCl unit cell,[19] it is highly likely that other ordering regimes are possible, for different stoichiometries, cation charges and synthesis conditions. For example, Ji *et al.* report short-range ordering in two other nominally disordered rocksalts Li$_{1.2}$Mn$_{0.4}$Ti$_{0.4}$O$_2$ (LMTO) and Li$_{1.2}$Mn$_{0.4}$Zr$_{0.4}$O$_2$ (LMZO) as taking the form of cubic α-LiFeO$_2$ (rather than tetragonal) units and tetrahedral cation clusters respectively, albeit with a much shorter correlation length (less than 10 Å).[15] As Ji *et al.* report, this ordering (or lack thereof) has implications for the electrochemical performance of LNbMO as a potential cathode material. Lee *et al.* attribute facile Li diffusion in disordered Li-excess materials to the percolation of 0-TM channels (networks of coordination environments where Li can diffuse between octahedral sites via tetrahedral sites with no TM neighbours).[25] γ-LiFeO$_2$ has entirely 2-TM channels, and hence has a much higher barrier to Li-diffusion throughout the structure. A 45% excess of Li is required to achieve percolation
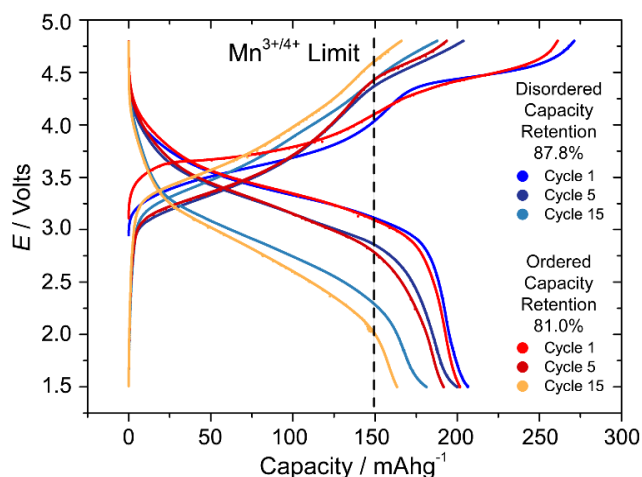
Figure 4. Electrochemical cycling data for disordered (blue) and ordered (red) LNbMO. Capacity retention values quoted are after 15 charge/discharge cycles. Both samples exhibit reversible redox beyond that possible from purely $Mn^{3+/4+}$ redox.

of 0-TM channels for the fully ordered γ-$LiFeO_2$ structure, and for 25% excess Li (i.e. $Li_{1.25}Nb_{0.25}Mn_{0.5}O_2$) > 25% cation mixing between sublattices is necessary to enable the lower activation energy diffusion pathways.[26] Indeed, electrochemical cycling data [Fig. 4] for LNbMO shows the more ordered material to suffer from greater voltage fade and poorer capacity retention. While both samples initially exhibit similar reversible capacities of over 200 mAhg^{-1}, the capacity retention after 15 cycles is significantly lower for the ordered material—81.0% compared with 87.8%. This ordering also appears to be lost after cycling [Fig. S6, ESI], in keeping with Kan *et al.*'s recent report on a Ta-containing analogue.[27]

In conclusion, we have proposed an ordering regime which accounts for extra superstructure reflections observed in $Li_{1.25}Nb_{0.25}Mn_{0.5}O_2$ using X-ray and neutron diffraction. The ordering is in keeping with the principle of electroneutrality and the specific stoichiometry of the material, and has been observed in similar rocksalt systems such as γ-$LiFeO_2$. The correlation length of these short-range correlations is dependent on the post-synthesis cooling rate, with rapid cooling leading to a shorter correlation length as might be expected on thermodynamic grounds. Magnetic susceptibility and NMR data for both longer and shorter correlation length samples of LNbMO are in agreement with the differences in local structure deduced from diffraction data. Understanding the local structure of these rocksalt systems—and how it can be controlled—is critical if they are to compete with current commercial cathode materials.

Conflicts of interest

There are no conflicts to declare.

References

1   P. Rozier and J. M. Tarascon, *J. Electrochem. Soc.*, 2015, **162**, A2490–A2499.
2   N. Yabuuchi, M. Takeuchi, M. Nakayama, H. Shiiba, M. Ogawa, K. Nakayama, T. Ohta, D. Endo, T. Ozaki, T. Inamasu, K. Sato and S. Komaba, *Proc. Natl. Acad. Sci. U. S. A.*, 2015, **112**, 7650–7655.
3   D. H. Seo, J. Lee, A. Urban, R. Malik, S. Kang and G. Ceder, *Nat. Chem.*, 2016, **8**, 692–697.
4   B. Li and D. Xia, *Adv. Mater.*, 2017, **1701054**, 1–28.
5   M. K. Aydinol, A. F. Kohan, G. Ceder, K. Cho and J. Joannopoulos, *Phys. Rev. B*, 1997, **56**, 1354–1365.
6   W.-S. Yoon, C. P. Grey, M. Balasubramanian, X.-Q. Yang, D. A. Fischer and J. McBreen, *Electrochem. Solid-State Lett.*, 2004, **7**, A53.
7   J. Lee, D.-H. Seo, M. Balasubramanian, N. Twu, X. Li and G. Ceder, *Energy Environ. Sci.*, 2015, **8**, 3255–3265.
8   N. Yabuuchi, *Chem. Lett*, 2017, **412**, 412–422.
9   N. Yabuuchi, M. Takeuchi, M. Nakayama, H. Shiiba, M. Ogawa, K. Nakayama, T. Ohta, D. Endo, T. Ozaki, T. Inamasu, K. Sato and S. Komaba, *Proc. Natl. Acad. Sci.*, 2015, **112**, 7650–7655.
10   N. Yabuuchi, M. Nakayama, M. Takeuchi, S. Komaba, Y. Hashimoto, T. Mukai, H. Shiiba, K. Sato, Y. Kobayashi, A. Nakao, M. Yonemura, K. Yamanaka, K. Mitsuhara and T. Ohta, *Nat. Commun.*, 2016, **7**, 13814.
11   R. Wang, X. Li, L. Liu, J. Lee, D. H. Seo, S. H. Bo, A. Urban and G. Ceder, *Electrochem. commun.*, 2015, **60**, 70–73.
12   W. H. Kan, D. Chen, J. K. Papp, A. K. Shukla, A. Huq, C. M. Brown, B. McCloskey and G. Chen, *Chem. Mater.*, 2018, **30**, 1655–1666.
13   C. Zhan, Z. Yao, J. Lu, L. Ma, V. A. Maroni, L. Li, E. Lee, E. E. Alp, T. Wu, J. Wen, Y. Ren, C. Johnson, M. M. Thackeray, M. K. Y. Chan, C. Wolverton and K. Amine, *Nat. Energy*, 2017, **2**, 963–971.
14   K. Luo, M. R. Roberts, R. Hao, N. Guerrini, D. M. Pickup, Y.-S. Liu, K. Edström, J. Guo, A. V. Chadwick, L. C. Duda and P. G. Bruce, *Nat. Chem.*, 2016, **8**, 684–691.
15   H. Ji, A. Urban, D. A. Kitchaev, D. Kwon, N. Artrith, C. Ophus, W. Huang, Z. Cai, T. Shi, J. C. Kim, H. Kim and G. Ceder, *Nat. Commun.*, 2019, **10**, 1–9.
16   W. H. Kan, B. Deng, Y. Xu, B. Wang, Y. Liu and G. Chen, *Chem*, 2018, **4**, 2108–2123.
17   H. T. Stokes, D. M. Hatch and B. J. Campbell, ISODISTORT, ISOTROPY Software Suite, iso.byu.edu.
18   B. J. Campbell, H. T. Stokes, D. E. Tanner and D. M. Hatch, 2006, **39**, 607–614.
19   G. C. Mather, C. Dussarrat, J. Etourneau and A. R. West, *J. Mater. Chem.*, 2000, **10**, 2219–2230.
20   A. Coelho, *TOPAS Academic, Version 6*, Coelho Software, Brisbane, Australia, 2007.
21   H. M. Rietveld, *J. Appl. Crystallogr.*, 1969, **2**, 65–71.
22   J. B. Goodenough, *J. Phys. Chem. Solids*, 1958, **6**, 287–297.
23   J. Kanamori, *Prog. Theor. Phys.*, 1957, **17**, 177–196.
24   D. Carlier, M. Ménétrier, C. P. Grey, C. Delmas and G. Ceder, *Phys. Rev. B*, 2003, **67**, 174103.
25   J. Lee, A. Urban, X. Li, D. Su, G. Hautier and G. Ceder, *Science*, 2014, **343**, 519–22.
26   A. Urban, J. Lee and G. Ceder, *Adv. Energy Mater.*, 2014, **4**, 1–9.
27   W. H. Kan, C. Wei, D. Chen, T. Bo, B. T. Wang, Y. Zhang, Y. Tian, J. S. Lee, Y. Liu and G. Chen, *Adv. Funct. Mater.*, 2019, **29**, 1–11.
28   I. Hung, L. Zhou, F. Pourpoint, C. P. Grey and Z. Gan, *J. Am. Chem. Soc.*, 2012, **134**, 1898–1901.